Dendritic Cells and Monocyte/Macrophages That Create the IL-6/APRIL-Rich Lymph Node Microenvironments Where Plasmablasts Mature[1]

Elodie Mohr,[2]* Karine Serre,* Rudolf A. Manz,† Adam F. Cunningham,* Mahmood Khan,* Deborah L. Hardie,* Roger Bird,* and Ian C. M. MacLennan*

IL-6 and APRIL influence the growth, differentiation, and survival of normal and neoplastic Ab-forming cells (AFC). In this study, we identify two subsets of myeloid cells that associate with the AFC and are the main producers of these factors during a T-dependent Ab response to alum-precipitated protein in mouse lymph nodes. First $CD11c^+CD8\alpha^-$ dendritic cells located in the perivascular area of the T zone provide about half of the IL-6 mRNA produced in the node together with significant amounts of APRIL mRNA. The number of these cells increases during the response, at least in part due to local proliferation. The second subset comprises $Gr1^+CD11b^+F4/80^+$ monocyte/macrophages. These colonize the medullary cords during the response and are the other main IL-6 mRNA producers and the greatest source of APRIL mRNA. This medullary cord monocyte/macrophage subset results in local increase of APRIL mRNA that mirrors the polarity of CXCL12 expression in the node. The distribution of these myeloid cell subsets correlates with a gradient of AFC maturation assessed by progressive loss of Ki67 as AFC pass from the B cell follicle along the perivascular areas to the medullary cords. *The Journal of Immunology,* **2009, 182: 2113–2123.**

During T-dependent Ab responses in lymph nodes (LN)[3] or the spleen, B cells that specifically bind Ag migrate to the outer T zone. In this compartment, cognate interaction with primed CD4 T cells results in formation of B blasts that either directly differentiate into plasmablasts in the outer T zone or migrate to B cell follicles where they form germinal centers (GC). In GC, the B blasts undergo affinity maturation through somatic hypermutation followed by selection based on Ag and T cell recognition (1–3). A proportion of the selected cells become plasmablasts that pass through the outer T zone. In the LN, many plasmablasts continue on to the medullary cords where they become plasma cells that secrete high levels of Ab and die in situ (4). Other plasmablasts leave the node and migrate to long-lived plasma cell-sustaining microenvironments in the bone marrow (5–7). This study concerns the nature of the microenvironments in LN, through which plasmablasts migrate and mature to become plasma cells. Plasmablasts and plasma cells are referred to collectively as Ab-forming cells (AFC).

The number of Ag-specific B cells recruited into the response directly influences the number of plasmablasts formed. In contrast, the proportion of plasmablasts that mature to become plasma cells is limited by the microenvironments occupied by these cells. If more plasmablasts are produced than can be sustained by these microenvironments the excess cells die (8–10).

In vitro and in vivo studies have identified a number of factors that influence plasmablast growth, maturation, and survival. Among these factors are IL-6 (11–13), the chemokine CXCL12 (12), and the TNF family factors TNF-α (12), B cell-activating factor (BAFF), and a proliferation-inducing ligand (APRIL) (14–17). In addition, CD44 (12) and VLA-4 (11) cross-linking affects these processes. These same factors are also involved in the survival of neoplastic Ab-secreting cells and plasma cells in autoimmune diseases (18–21). Thus, identification of the source of these factors may have considerable impact for the understanding of the development of Ab responses and the treatment of these diseases.

The objective of the present study has been to identify and characterize the cells associated with plasmablasts and plasma cells that produce these factors. To complete our objective, confocal microscopy was used to identify AFC-associated cells in the LN of mice immunized s.c. with the T-dependent Ag, aluminum hydroxide (alum)-precipitated (4-hydroxy-3-nitrophenyl) acetyl (NP)-OVA (alumNP-OVA). Different myeloid cell types were identified in these microenvironments and flow cytometric analysis shows that the number of these cells increases dramatically during the Ab response, as the AFC are produced. The relative contribution of each of the FACS-sorted AFC-associated myeloid cell subsets to the production of factors known to influence plasmablast growth, maturation, and survival within the node was determined using real-time RT-PCR. This analysis shows that high producers of APRIL and IL-6 mRNA colocalize with AFC. Finally, laser microdissection of histologically defined areas in the node combined with real-time RT-PCR reveals that the presence of AFC-associated myeloid cells in the medulla results in local enrichment in APRIL mRNA. This higher production in the CXCL12-rich medullary cords correlates with the accumulation of $CXCR4^+$ mature

*Medical Research Council Centre for Immune Regulation, University of Birmingham Medical School, Birmingham, United Kingdom; and †Department for Humoral Immunology, German Arthritis Research Centre, Berlin, Germany

Received for publication August 25, 2008. Accepted for publication December 15, 2008.

The costs of publication of this article were defrayed in part by the payment of page charges. This article must therefore be hereby marked *advertisement* in accordance with 18 U.S.C. Section 1734 solely to indicate this fact.

[1] This work was funded by a programme grant from the British Medical Research Council. R.A.M. is supported by a Deutsche Forschungsgemeinschaft Grant MA 2273/4-2.

[2] Address correspondence and reprint requests to Dr. Elodie Mohr, Medical Research Council Centre for Immune Regulation, Room 435, Institute of Biomedical Research building, University of Birmingham Medical School, Vincent Drive, Birmingham B15 2TT, U.K. E-mail address: e.mohr@bham.ac.uk

[3] Abbreviations used in this paper: LN, lymph node; AFC, Ab-forming cell; DC, dendritic cell; BAFF, B cell-activating factor; GC, germinal center; APRIL, a proliferation-inducing ligand; alumNP-OVA, aluminum hydroxide-precipitated (4-hydroxy-3-nitrophenyl) acetyl ovalbumin.

www.jimmunol.org/cgi/doi/10.4049/jimmunol.0802771

plasma cells transcribing high levels of two APRIL receptors, TACI (transmembrane activator and calcium-modulator and cyophilin ligand interactor) and BCMA (B cell maturation Ag).

Materials and Methods

Mice, adoptive transfer, immunization and BrdU injection

Wild-type C57BL/6J mice 5–7 wk of age were purchased from Harlan OLAC. For adoptive transfer, 5×10^6 cells from LN of OT-II mice, transgenic for $\alpha\beta$ TCR specific for $OVA_{323-339}$ peptide in the context of H-2 $I\text{-}A^b$ (Charles River Breeding Laboratories) were injected i.v. into wild-type C57BL/6J recipients. Mice were immunized the following day with alumNP-OVA. To make alumNP-OVA, (4-hydroxy-3-nitrophenyl) acetyl-OVA protein (Biosearch Technologies) was mixed with a 9% aluminum potassium sulfate solution (Sigma-Aldrich). In a final volume of 10 μl in PBS, 10 μg of alumNP-OVA was injected s.c. into the footpad of the rear feet. BrdU (2 mg) in PBS was injected i.p. 6 h before sacrifice. All animals were maintained under standard animal housing conditions in accordance with local and home office regulations.

Confocal microscopy, microdissection, and Giemsa-Grünwald staining

Each staining was done on at least three LN each harvested in independent experiments. Popliteal LN were embedded in Tissue-Tek OCT compound (Sakura) and snap frozen in liquid nitrogen, and 6-μm sections were cut on a cryostat. Sections were dried at room temperature for 1 h, fixed in acetone for 20 min, and dried for 10 min. Staining was performed in PBS containing 10% FCS, 0.1% azide and sections were mounted in 2.5% 1,4-Diazabicyclo (2,2,2)octane (pH 8.6) in 90% glycerol in PBS. Primary and secondary Abs are listed (see Supplemental Table I).[4] Confocal images were acquired using a Zeiss LSM510 laser scanning confocal microscope with a Zeiss AxioVert 100M microscope equipped with 10X and 63X objectives. FITC- or Alexa Fluor 488-labeled reagents were excited with a 488 nm argon laser; TRITC, Alexa Fluor 546, or Cy3 conjugates were excited with a 543 nm HeNe laser; allophycocyanin, Alexa Fluor 633, or Cy5 conjugates were excited with a 633 nm helium laser; and aminomethylcoumarin acetate or Alexa Fluor 350 were excited with 351/364 nm lasers. Signals obtained from these four lasers were scanned separately and stored in four nonoverlapping channels as pixel digital arrays of 2048 $\times$ 2048 (when taken with the 10X objective) or 1024 $\times$ 1024 (when taken with the 63X objective).

For microdissection, LN were processed as described, but serial sections were collected on PALM MembraneSlides NF and stained for 3 min with 1% w/v cresyl violet (Sigma-Aldrich) in ethanol after hydration in 100%, 70%, and 50% ethanol. Slides were then washed again quickly in 50%, 70%, 100% ethanol sequentially and air-dried. Laser microcapture was performed using a Microbeam HT microscope (PALM Microlaser Technologies). The 20–40 microdissected similar areas were catapulted into RNeasy buffer (Qiagen) and processed as described for RT-PCR.

$Gr1^{int}CD11b^{high}F4/80^+$ or $Gr1^{high}CD11b^{high}F4/80^-$ cells were sorted and plated using cytospin centrifugation 5 min at 350 rpm, fixed 10 min in methanol, slightly dried, stained 5 min with 33% v/v Grünwald solution in 4 mM (pH 5.6) phosphate buffer, washed once in phosphate buffer, stained with 10% v/v Giemsa R66 Gurr solution (BDM Laboratory Supplies) in phosphate buffer, and washed off with phosphate buffer. After drying, slides were mounted in Depex medium (Gurr).

Flow cytometric analysis and FACS Cell Sort

The LN fragments were digested (except for CD138 or CXCR5 staining) for 20 min at room temperature with 1 mg/ml collagenase type II (Lorne Laboratories) and 0.15 mg/ml DNase I (Sigma-Aldrich), and then treated (except for 33D1 staining) for 5 min with 10 mM EDTA (Sigma-Aldrich). For myeloid cells, 10-min incubation on ice with supernatant from 2.4G2 hybridoma culture and 5% normal mouse serum were added. Cells were stained in 2 mM EDTA-PBS supplemented with 0.1% FCS. Intracellular FACS staining was performed using Cytofix/Cytoperm kit (BD Biosciences) and BrdU was detected with BrdU APC flow kit (BD Biosciences). (For Ab references see Supplemental Table I.[4]) Cells were sorted using a FACS (MoFlow; DakoCytomation). Analysis by flow cytometry of LN cell suspensions or purity assessment of sorted cells was done using a FACSCalibur (BD Biosciences). Final analysis and graphical output were performed using FlowJo software (Tree Star).

[4] The online version of this article contains supplemental material.

Real-time RT-PCR

mRNA was extracted using RNeasy columns from Qiagen. Reverse transcription was performed with random oligonucleotides (Promega) using Moloney Murine Leukemia Virus reverse transcriptase (Invitrogen) for 1 h at 42°C. Relative quantification of specific cDNA species was calculated by referring to the β-actin or β_2-microglobulin mRNA levels, quantified in a duplex PCR on ABI 7900 using TaqMan chemistry (Applied Biosystems). When not compatible in duplex, target and reference genes were measured in simplex real-time PCR run simultaneously for the same sample. Probes for target genes were detected via a 5′ label with FAM, whereas probe for β-actin or β_2-microglobulin were 5′ labeled with VIC or Yakima Yellow (Applied Biosystems). TaqMan probes and primers (see Supplemental Table II)[4] were designed by using Primer Express computer software (Applied Biosystems) and synthesized by Eurogenetec. Standard reaction conditions for the TaqMan PCR were used. For each gene assessed, the relative contribution of each cell subset to the total amount produced within the total cell suspension in day 8 LN (100%) was estimated by multiplying its average expression by the average number of cells (see Fig. 6 pie charts). The redundancy due to the expression of $CD11c^{int}$ by a known proportion of $CD169^+$ and $Gr1^+$ cells (see Supplemental Table III)[4] was suppressed by subtracting the amounts of mRNA produced by $CD11c^{int}CD169^+$ and $CD11c^{int}Gr1^+$ cells from those obtained for the $CD11c^{int}$ cells.

Results

The AFC production and characteristics during the T-dependent response to alumNP-OVA in LN

The kinetics of AFC production was assessed in the draining popliteal LN following footpad immunization with alumNP-OVA. This response is a Th2-dependent primary Ab type and to increase the B cell response mice received naive OVA-specific CD4 T cells (OT-II cells) i.v. 24 h before immunization. AFC, identified as $CD138^+$ cells, appeared from 3 days after immunization, and IgG1-secreting cells were first detected between days 4 and 5 (Fig. 1*A*). The peak of the AFC response was at day 8, when 80% of the AFC had switched to IgG1 and AFC comprised some 2% of LN cells (Fig. 1*A*, graph). During the second and third weeks of the response, AFC numbers in the draining LN fell progressively.

The expression of cell surface molecules associated with AFC localization, differentiation, growth, and survival was assessed. This expression is shown in Fig. 1, *B* and *C*, where the phenotype of $CD138^+$ AFC isolated at day 8 of the response to alumNP-OVA is compared with that of $B220^+IgM^+$ B cells from the LN of nonimmunized mice. As expected MHC class II, CD40, IL-4R α-chain (CD124), and CXCR5 expressed by the naive B cells were down-regulated in AFC (Fig. 1*B*). By contrast AFC had up-regulated their surface expression of CXCR4, CD54, CD18, CD11a, CD49d, and CD44 (22). There were major increases in the level of transcripts of the two TNFR family members, TACI and BCMA, which bind both APRIL and BAFF factors implicated in AFC growth and survival (Fig. 1*C*). TACI mRNA in AFC was increased 15-fold and BCMA mRNA 2500-fold. By contrast no variation in the BAFF receptor BAFF-R mRNA was observed in AFC as compared with naive B cells.

The location of AFC related to their proliferation

By day 8 of the response, AFC are located at the outer edge of the T zone and in the medullary cords (Fig. 2A). In the outer T zone the AFC are seen adjacent to secondary follicles as well as in the vicinity of high endothelial venules ($PNAd^+$) and intranodal lymphatic vessels ($Lyve\text{-}1^+$). A high proportion of the AFC in the parts of the T zone adjacent to GCs are in cell cycle, as assessed by the expression of Ki67 (Fig. 2*B*, B1). By contrast, fewer AFC in the medullary cords are $Ki67^+$ but these produce higher levels of Ig as seen by increased intensity in IgG1 staining (Fig. 2*B*, B2). Fig. 2*C* shows quantification of the proportion of AFC that are positive for Ki67 as a function of their distance from the follicles.

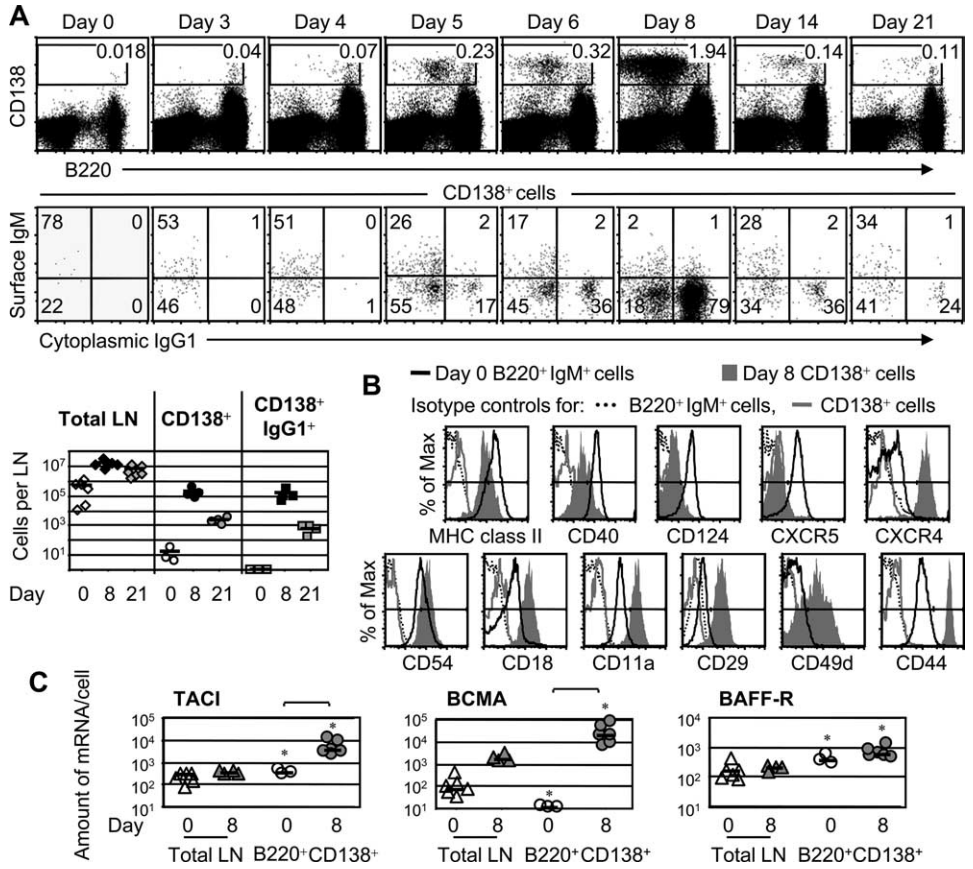

FIGURE 1. The rate of production and characteristics of AFC responding to alumNP-OVA in LN. *A*, Kinetics of $CD138^+$ cell production in draining LN during the first 3 wk after footpad immunization with 10 μg of alumNP-OVA (*top row*). The proportion of LN cells in the $CD138^+$ gate is shown, as well as the proportion of $CD138^+$ cells positive for cytoplasmic IgG1 and surface IgM (*bottom row*). These results are representative of three independent similar experiments involving $n = 1$ or 2 mice per time point. The absolute number of these cells is shown (*lower left chart*). Each symbol represents the results from one LN from $n = 1$ mouse. *B*, Representative flow cytometric analysis of the phenotype of $CD138^+$ cells obtained from day-8 LN (filled histograms) compared with that of resting $B220^+IgM^+$ B cells from day-0 LN (open histograms). *C*, Transcription of TNFR family member genes BAFF-R, TACI, and BCMA during AFC differentiation, quantified by real-time RT-PCR and normalized according to the β-actin level. Resting $B220^+$ cells from nonimmunized mice are compared with AFC ($CD138^+$ cells) FACS sorted at day 8 postimmunization. Background levels of expression were obtained from total cell suspensions from nonimmunized and day-8 postimmunized LN. Each symbol represents an independent experiment, in which cells were isolated from the four popliteal LN of $n = 2$ mice. Horizontal bar shows geometric mean. Statistical significance was assessed by *t* test. *, $p < 0.05$ significant difference, as compared with the level obtained in total LN at the corresponding time point. Upper line links populations displaying a significant difference of $p < 0.05$.

There is a consistent and highly significant reduction in the proportion of AFC that are $Ki67^+$ among cells in the medulla compared with those adjacent to the follicles. This observation is in keeping with progressive maturation, in which the recently produced plasmablasts occupy the area close to the follicles, whereas mature postmitotic AFC accumulate in the medullary cords.

We next identified the cells associated with AFC and the growth, differentiation, and survival factors they produce. These are divided into the following three mutually exclusive groups: 1) $CD11c^+$, 2) $CD169^+$ and 3) $Gr1^+$ populations that are each detailed in an individual section of the results.

Subsets of $CD11c^+$ dendritic cells (DC) associated with AFC

Earlier work has shown that $CD11c^{high}$ cells with dendritic morphology colocalize with AFC in the spleen and LN immunized during both T-independent and T-dependent Ab responses (9, 10). Importantly, agonistic anti-CD40 treatment of the immunized mice resulted in dramatic augmentation of both AFC and $CD11c^{high}$ DC. The $CD11c^+$ cells display diverse phenotypes that reflect different functions (23). In the present study, we defined four nonoverlapping subsets based on the level of CD11c expression and whether the cells expressed CD8α or F4/80 (Fig. 3, *A* and *B*). Three of the subsets were $CD8\alpha^-$, including $CD11c^{high}F4/80^+$, $CD11c^{high}F4/80^-$, and $CD11c^{int}CD8\alpha^-$ (referred to as $CD11c^{int}$), and a fourth subset was $CD8\alpha^+$ ($CD11c^+CD8\alpha^+$). Each of these $CD11c^+$ cells have features associated with presentation of Ag and costimulation of CD4 T cells, i.e., class II MHC, CD40, CD80, and CD86 (see Supplemental Table III),[4] and on this basis they will be referred to as DC.

AFC in the outer T zone, as opposed to the medulla, were particularly associated with $CD11c^{high}CD8\alpha^-$ DC. These cells were found both at the interface between the T zone and secondary follicles as well as along the vessels that connect the subcapsular sinus with the medullary lymphatics (Fig. 3*A*, A1). In addition some $CD11c^+CD8\alpha^+$ DC were seen adjacent to AFC in these outer T zone areas. Few $CD11c^{high}CD8\alpha^-$ cells were found in the medullary cords (Fig. 3*A*, A2). Some $CD11c^{int}$ cells were also found associated with AFC in the outer T zone (Fig. 3*A*, A1), and in contrast to other $CD11c^+$ subsets, some $CD11c^{int}$ cells were also seen the medullary cords (Fig. 3*A*, A2). Although F4/80-expressing cells associated with plasmablasts in the outer T zone were mainly $CD11c^+$ DC (Fig. 3*B*, B1), a majority of the $F4/80^+$

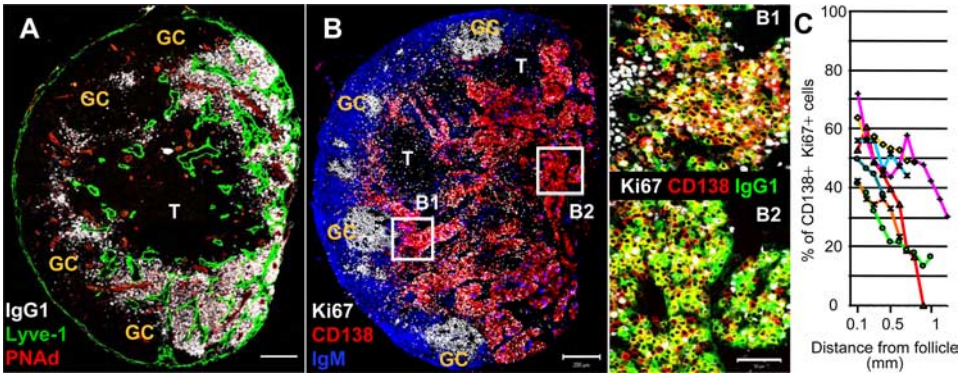

FIGURE 2. The location of AFC related to their proliferation. *A*, Composite confocal images of day 8 LN showing IgG1$^+$ cells (white) adjacent to high endothelial venules (red; peripheral node addressin (PNAd)) and intranodal lymphatics (green; Lyve-1). The location of GC is indicated; the center of T zone area (T) is also marked. *B*, Confocal images of a serial section to *A* showing the location of CD138$^+$ cells (red) and IgM$^+$ follicle mantle cells (blue). The follicles contain GC with Ki67$^+$ cells (white). B1 and B2 are re-imaged at a higher magnification (*inset*) to show IgG1 (green) in addition to Ki67 (white) and CD138 (red). In B1, a perifollicular area of outer T zone, many of the CD138$^+$ cells are Ki67$^+$ and have low IgG1 expression and appear in red. Conversely in B2, an area of medulla, most of the CD138$^+$ cells are Ki67$^-$ and produce IgG1 (yellow). White scale bar on the confocal image represents 200 μm (*A* and *B*) and 50 μm in B2. *C*, The proportion of CD138$^+$ cells in cell cycle related to their distance from the follicles. Concentric lines were drawn at 100-μm intervals on the T zone side of a line drawn along the B-T boundary. The proportion of CD138$^+$ cells that were Ki67$^+$ was quantified for the cells between adjacent lines. Each curve represents the values obtained from one LN section in one of seven independent experiments. The proportion of CD138$^+$ Ki67$^+$ cells in all seven LN sections falls from the 100 μm adjacent to the follicles to the 100 μm in the medulla. $*$, $p < 0.0006$ by two-tailed Mann-Whitney nonparametric statistics.

cells adjacent to plasma cells in the medulla are CD11c$^-$ macrophages (Fig. 3*B*, B2). These are considered below.

Between days 0 and 8 after immunization, whereas CD11c$^+$CD8α^+ and CD11c^{int} cells as a percentage of total LN cells remained constant, the percentage of CD11c^{high} cells increased (Fig. 3*C*). Nevertheless, as the total number of cells in the LN increased by 20-fold on average (Fig. 1*A*, graph under dot plots), the absolute number of all subsets of CD11c$^+$ cells increased (Fig. 3*D*, graph at *left*). This particularly applied to the CD11c^{high}F4/80$^+$ subset that increased by around 30-fold by day 8 after immunization (Fig. 3*D*). This enrichment in all the CD11c$^+$ DC populations in the LN was due, at least in part, to proliferation; a proportion of these cells incorporated BrdU given i.p. 6 h before the LN were taken on day 8. The number of cells that had incorporated the label within each subset of CD11c$^+$ DC had at least doubled compared with nonimmunized LN (Fig. 3*D*, *right*).

The phenotypic comparison of the CD11c$^+$ subsets was extended (see Supplemental Table III).[4] Interestingly, 30% of CD11c^{high}F4/80$^+$ cells expressed high level of CXCR4, whereas none expressed CXCR5. This property may be responsible for CD11c^{high}F4/80$^+$ cells colocalizing with AFC at the edges of the T zone. Coexpression of ICAM-1 and VCAM-1 by some of these cells may also play a part in their localization and cellular interactions with AFC.

CD169$^+$ cells associated with AFC in the outer T zone differ in phenotype from those in the medulla

As seen in the previous section, F4/80$^+$ cells with the macrophage-associated feature of low or no CD11c expression are seen in close association with AFC in the medullary cords. A possible role in AFC differentiation for CD169 (sialoadhesin), a protein expressed on subsets of macrophages, was suggested from studies of CD169-deficient mice; these mice have reduced serum IgM levels while having an apparently normal number of mature B cell subsets (24). Thus, F4/80$^+$CD11c$^{low/-}$ cells were assessed for their expression of CD169, among other macrophage markers. Consistent with a role of CD169$^+$ cells in AFC growth or maturation, we found cells in the medullary cords with macrophage morphology that were CD169$^+$CD11b$^+$F4/80$^+$. These were located along the edge of AFC clusters (Fig. 4*A*, A2), in close association with the lymphatic endothelium that surrounds the medullary cords (data not shown). By contrast, the CD169$^+$CD11b$^+$ cells that did not express F4/80 were associated with AFC in the outer T zone (Fig. 4*A*, A1). Lastly, CD169$^+$ macrophages negative for both CD11b and F4/80 were found in the wall of the subcapsular sinus. These are likely to be the cells associated with capturing and transporting Ag from the lymph to B cells underlying the sinus (25, 26). Although on tissue section all subsets of CD169$^+$ cells appeared negative for CD11c, analysis by flow cytometry indicates that these cells express this integrin at various levels (see Supplemental Table III).[4] Some CD169$^+$ cells in nonimmunized LN expressed low levels of Gr1, a marker of granulocytes, monocytes, and immature macrophages, but by day 8 the CD169$^+$ cells were negative for Gr1 (Fig. 4*B*). Gr1$^{high/int}$ cells are considered below.

The proportion of CD169$^+$ cells among LN cells was reduced by day 8, particularly the CD169$^+$CD11b$^+$F4/80$^{+/-}$ cells associated with AFC (Fig. 4*B*). Nevertheless, the absolute number per node of all three CD169$^+$ cell subsets (CD169$^+$CD11b$^+$F4/80$^+$, CD169$^+$CD11b$^+$F4/80$^-$, and CD169$^+$CD11b$^-$F4/80$^-$) increased between days 0 and 8 (Fig. 4*C*). This response was associated with some proliferation, for 15% of CD169$^+$ cells were found to have incorporated BrdU (Fig. 4*C*, *right*).

Consistent with their localization with AFC in the outer T zone and the medullary cords, more CD169$^+$CD11b$^+$F4/80$^-$ and CD169$^+$CD11b$^+$F4/80$^+$ cells expressed CXCR4 than CXCR5 (see Supplemental Table III).[4] Of note, CXCL12 chemokine, the ligand for CXCR4, was also detected in some CD169$^+$ macrophages interacting with IgG1$^+$ AFC (Fig. 4*D*) (also seen in Fig. 6). Finally, CD169$^+$CD11b$^+$F4/80$^-$ and CD169$^+$CD11b$^+$F4/80$^+$ expressed high levels of the adhesion molecules VCAM-1, ICAM-1, and CD49d, which may assist in their colocalization and interaction with AFC.

Gr1$^+$CD11b^{high} neutrophils and monocyte/macrophages colocate with medullary AFC

A subset of CD11b$^+$F4/80$^+$ cells that were negative for CD169 were found among the AFC in the medullary cords (magenta cells in Fig. 4*A*, A2). Cells with this phenotype have been described that

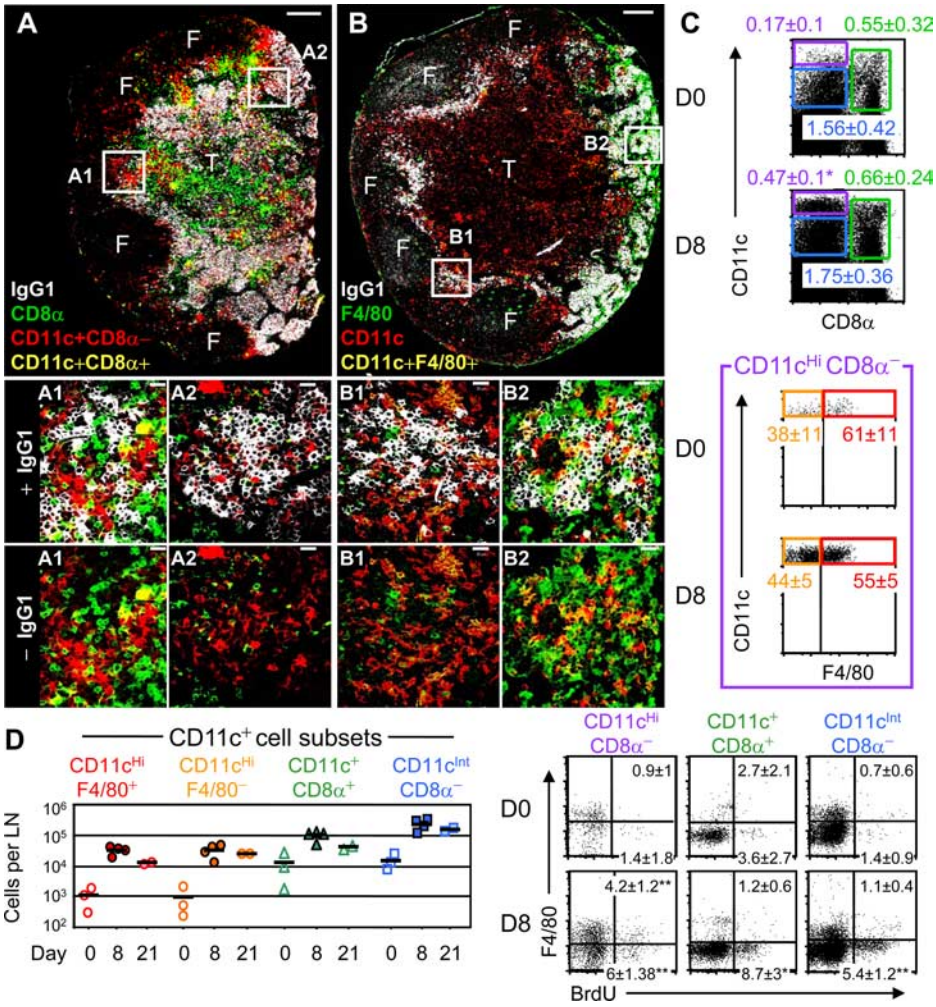

FIGURE 3. Characteristics of CD11c$^+$ DC subsets associated with AFC. *A* and *B*, Composite confocal images of a day-8 LN section. *A*, CD11c$^+$CD8α^- cells (red) are associated with IgG1$^+$ cells (white) in the outer T zone (A1) and surround clusters of plasma cells in the medullary cords (A2). Only a small proportion of the CD11c$^+$CD8α^+ DC (yellow) are found close to IgG1$^+$ cells. Follicles (F) and T zone (T) areas are shown. *B*, CD11c^{high}F4/80$^+$ cells (yellow) that colocalize with IgG1$^+$ cells (white), both in the perifollicular T zone (B1) and the medullary cords (B2). These two AFC-rich environments are markedly different, for although CD11c^{high} and CD11c^{int} cells (red or yellow) are frequent in the outer T zone (B1), F4/80$^+$CD11c$^-$ macrophages (green) are predominant in the medulla (B2). White scale bar on confocal images represents 200 μm (*A* and *B*), and 20 μm in A1, A2, B1, and B2. *C*, Flow cytometric analysis of the different subsets of CD11c$^+$ DC in day-0 and day-8 LN. Four populations of CD11c$^+$ DC, as defined by confocal immunohistology in *A* and *B* are considered. Percentage of CD11c^{high}CD8α^- (purple gate), CD11c$^+$CD8α^+ (green gate), and CD11c^{int}CD8α^- (blue gate) (*top plots*) is shown. CD11c^{high}CD8α^- cells comprise F4/80$^+$ (red gate) and F4/80$^-$ (orange gate) subsets (*bottom plots*). Dot plots are representative of LN populations obtained from $n = 8$ mice both at day 0 and day 8 studied in five independent experiments. The mean percentages and SD for the mice studied ($n = 8$) at each time are shown. *D*, The absolute number of cells with each phenotype per LN is shown (*left*) during the first 3 wk after alumNP-OVA. Each symbol represents cell number for one LN section for $n = 1$ mouse taken in one independent experiment. Dot plots (*right*) show BrdU incorporation during the 6 h before the cells were harvested by different populations of cells, in day 0 LN (*top row*) or day 8 LN (*bottom row*) and are representative of results obtained from $n = 9$ mice per time point studied in three independent experiments. Average percentage ± SD of BrdU$^+$ cells for mice ($n = 9$) in each group is indicated. Statistically significant variations in the proportion of different cell populations between days 0 and 8 (*C* and *D*) were assessed by Mann-Whitney nonparametric statistics. *, $p < 0.01$ and **, $p < 0.001$.

also express Gr1 (27) and Gr1$^+$CD11b$^+$ cells have been involved in supporting AFC growth (16, 28). The Gr1$^+$CD11b^{high} cells associated with AFC in the medullary cords were negative for two markers of plasmacytoid DC (29), namely B220 and CD11c (Fig. 5*A*, A1 and A2). In agreement with others (30) flow cytometry shows that two Gr1$^+$CD11b^{high} subsets are distinguishable based on Gr1 intensity and F4/80 expression. Gr1^{high}CD11b^{high}F4/80$^-$ cells displayed the morphology of neutrophils (Fig. 5*B*, dot plots (*left*) and stains (*top right*)), whereas Gr1^{int}CD11b^{high}F4/80$^+$ cells had a monocyte or macrophage appearance (Fig. 5*B*, dot plots (left) and stains (*bottom right*)). Some Gr1$^+$CD11b$^+$ cells have been shown to produce IL-4 during splenic immune responses to alum-precipitated protein (28), but no IL-4 mRNA was detected in the medullary Gr1$^+$CD11b$^+$ cells in the present study (data not shown). The IL-4-producing Gr1$^+$CD11b$^+$ cells reported by others may well be eosinophils (31) and display a selective tropism toward the spleen rather than the LN (32).

The intermediate Gr1 expression by CD11b^{high}F4/80$^+$ cells was not detectable by fluorescence microscopy. Therefore Gr1^{int} CD11b^{high}F4/80$^+$ cells were identified in tissue sections as CD11c$^-$ CD169$^-$CD11b^{high}F4/80$^+$ cells and found to be interspersed with AFC in the center of the medullary cords (Fig. 5*C*, C1). This approach was validated by FACS analysis that shows that these Gr1^{int} CD11b^{high}F4/80$^+$ cells were the only CD11c$^-$CD169$^-$CD11b^{high} F4/80$^+$ cells in LN (Fig. 5*D*). As with the other subsets associated with AFC, both types of Gr1$^+$CD11b^{high} cells preferentially

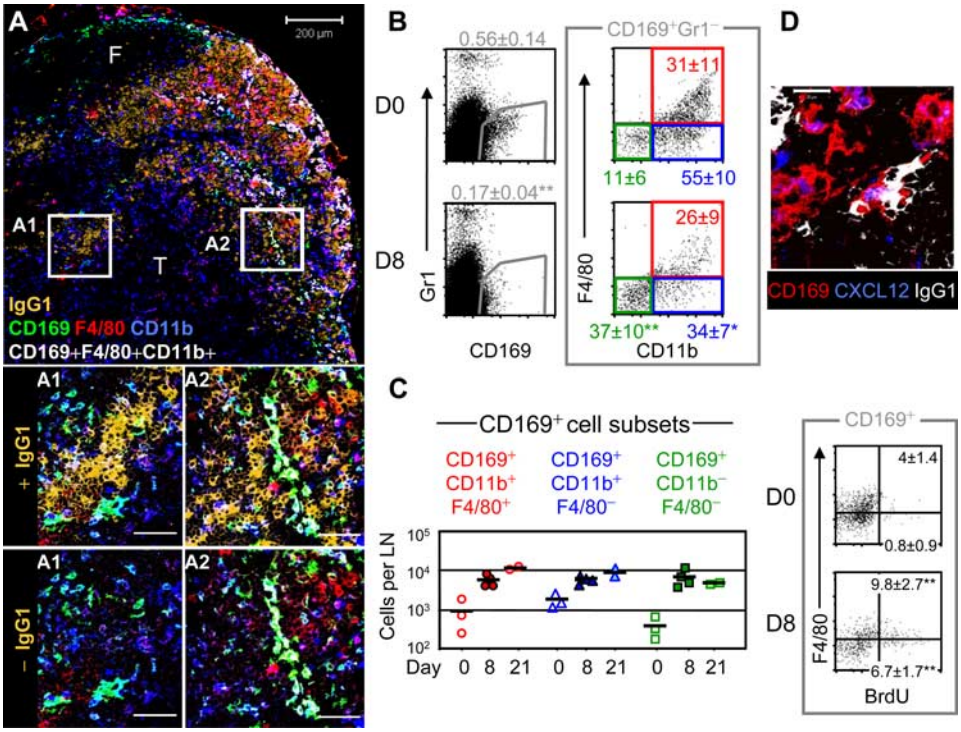

FIGURE 4. $CD169^+$ macrophages that interact with AFC display position-dependent phenotypes. *A*, Confocal image of day 8 LN section. $CD169^+$ cells (green) residing in the subcapsular sinus and the follicles (F) are $CD11b^-F4/80^-$. In the outer T zone (central T zone marked with (T)), $CD169^+$ cells coexpress $CD11b^+$ making them appear turquoise (A1), whereas in the medullary cords $CD169^+$ cells coexpress both F4/80 and CD11b giving a white appearance to part of each cell (A2). Both $CD169^+CD11b^+F4/80^+$ and $CD169^+CD11b^+F4/80^-$ subsets are in contact with $IgG1^+$ cells (orange). White scale bar on the confocal images represents 200 μm (*A*), and 50 μm in A1 and A2. *B*, $CD169^+$ macrophage subsets analyzed by flow cytometry in day 0 and day 8 LN. $CD169^+$ cells (gray gate) are $Gr1^-$ at day 8 and at best $Gr1^{low}$ on day 0. The proportion of $CD169^+CD11b^+F4/80^+$ (red gate), $CD169^+CD11b^+F4/80^-$ (blue gate), $CD169^+CD11b^-F4/80^-$ (green gate) cells is indicated. Dot plots are representative of LN populations obtained from $n = 9$ mice per time point studied in five independent experiments. Average percentage ± SD for all mice ($n = 9$) in each group is indicated. *C*, The absolute number of each subset of $CD169^+$ macrophages defined in *A* and *B* at days 0, 8, and 21. Each symbol represents the cell count for one LN section of $n = 1$ mouse taken in an independent experiment. Dot plots show BrdU incorporation by $CD169^+Gr1^-$ cells in the 6 h before the LN were taken. Dot plots are representative of results obtained from $n = 9$ mice per time point studied in three independent experiments. Average percentage ± SD of $BrdU^+$ cells for all mice ($n = 9$) in each group is indicated. *D*, Confocal image showing the interaction of $IgG1^+$ cells (white) with $CD169^+CXCL12^+$ cells (magenta) in a day-8 LN section. White scale bar represents 20 μm. Statistically significant variations in the proportion of different cell populations between day 0 and day 8 were assessed by Mann-Whitney nonparametric statistics. *, $p < 0.01$ and **, $p < 0.001$.

expressed CXCR4 without CXCR5, which is consistent with their absence from the follicles and their proximity to the AFC in the CXCL12-rich medullary cords (see Supplemental Table III).[4]

The number of $Gr1^{int}CD11b^{high}F4/80^+$ monocytes/macrophages cells increased 80-fold on average during the first 8 days after immunization, whereas the $Gr1^{high}CD11b^{high}F4/80^-$ neutrophils only increase by around 15-fold (Fig. 5*E*, *left*). These increases were not associated with BrdU incorporation during the last 6 h of the day 9 (Fig. 5*E*, *right*). Unless there was earlier proliferation, the increases must have been due either to recruitment of these cells into the node or differentiation in situ without cell division.

AFC-associated myeloid cells are the main producers of APRIL and IL-6 mRNA in the responding LN

The different myeloid cell subsets characterized in these experiments were assessed to see whether they produce one or more of the following factors associated with AFC differentiation or survival: APRIL, IL-6, BAFF, CXCL12, or TNF-α. Transcriptional levels per cell of these genes (related to the level of housekeeping genes) were quantified by real-time RT-PCR (Fig. 6, *left*). The mRNA levels in each FACS-sorted population before or 8 days after immunization were compared with the baseline expressions within total LN cell suspensions at the corresponding time.

Most of the AFC-associated cell subsets expressed APRIL, IL-6, and TNF-α at levels significantly above the baseline ($p < 0.05$). The estimation of the contribution of the different AFC-associated subsets to the total production of each of the factors within the responding node is represented in Fig. 6 (pie charts). (See *Materials and Methods* for the calculations used.) AFC-associated subsets are seen to be the main producers of APRIL and IL-6 in the day 8-immunized LN. Most of the IL-6 in the node is produced by $CD11c^+CD8\alpha^+$ and $CD11c^{int}$ subsets. In addition, cells in the $CD11c^{int}$ and $CD11c^+CD8\alpha^+$ subsets made a significant contribution to total APRIL mRNA in the LN. As the level per cell of the APRIL mRNA is lower in the $CD11c^+CD8\alpha^+$ DC, the efficiency of these cells in producing APRIL is less clear. The $CD11c^{high}F4/80^+$ DC closely associated with the AFC in the outer T zone produced IL-6 and APRIL mRNA at significant levels. Although they contributed modestly to the total amount of these mRNA transcribed in the LN, due to their privileged location these $CD11c^{high}F4/80^+$ DC are likely to provide effectively the AFC with these survival factors. Easily the highest levels of APRIL per cell were produced by the $Gr1^{int}CD11b^{high}F4/80^+$ cells that are located close to AFC in the medullary cords. Despite the relatively small total number of these cells, they were responsible for producing nearly half the APRIL mRNA in the node, making it likely this impacts on the plasma cells that surround them.

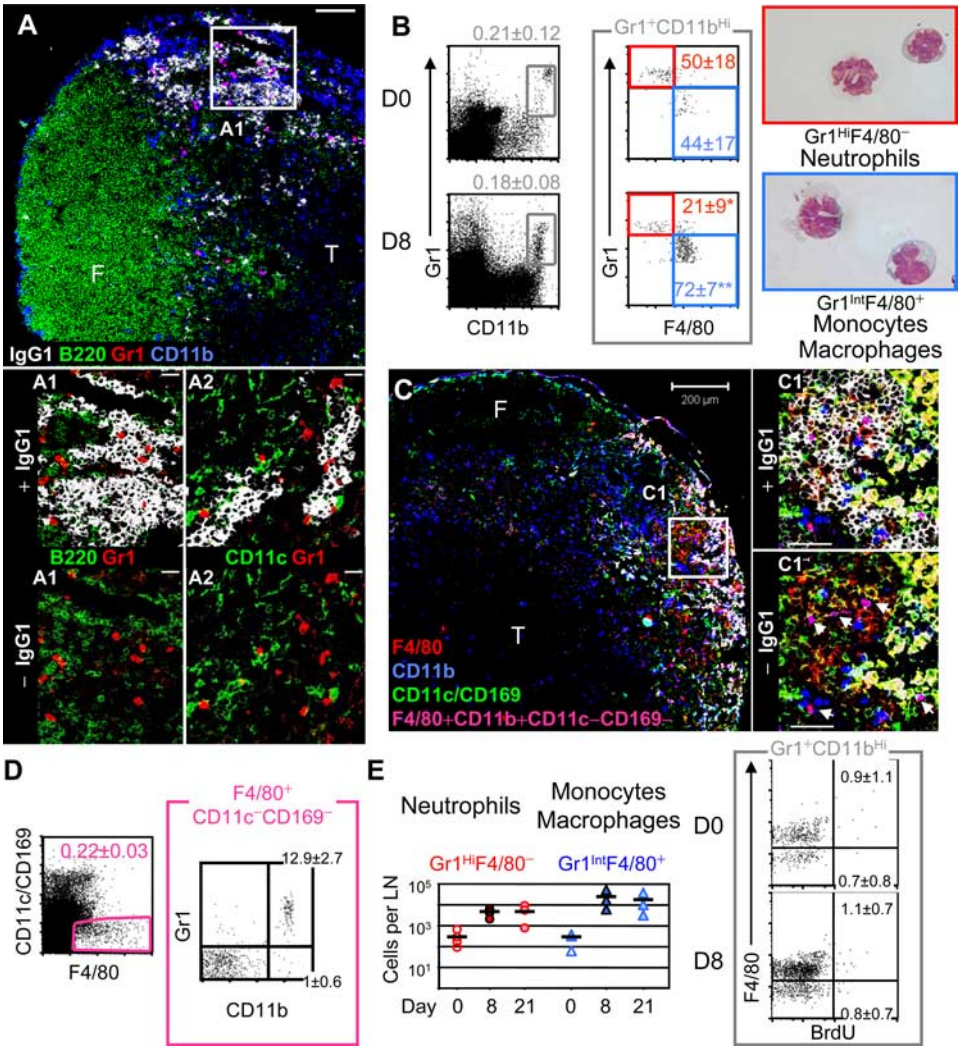

FIGURE 5. Gr1^{high}CD11b^{high} neutrophils and Gr1^{int}CD11b^{high}F4/80^{+} monocytes/macrophages colocalize with AFC in the medulla. *A*, Composite confocal image of day 8 LN section. IgG1^{+} AFC (white) colocalize, in the medullary cords, with magenta cells coexpressing Gr1^{+} (red) and CD11b^{high} (blue). Follicles are identified by B220 cells (green). In A1, higher magnification shows that Gr1^{+}CD11b^{high} cells (unlike plasmacytoid DC) are B220^{-}. In addition A2, taken from a serial section to *A*, shows that Gr1^{+}CD11b^{high} cells (red) do not express CD11c (green). White scale bar represents 100 μm in (*A*) and 20 μm in A1 and A2. *B*, Percentage of Gr1^{+}CD11b^{high} cells (gray gate) in day-0 and day-8 LN. Differential expression of F4/80 (*middle plots*) by Gr1^{high}CD11b^{high} cells, negative for F4/80 (red gate), and Gr1^{int}CD11b^{high} cells, positive for F4/80 (blue) is shown. Dot plots are representative of LN populations obtained from $n = 9$ mice per time point studied in four independent experiments. Mean percentage ± SD for all mice ($n = 9$) in each group is indicated. Light microscopy view of Giemsa-Grünwalt stained cytospins of FACS-sorted Gr1^{high}CD11b^{high}F4/80^{-} and Gr1^{int}CD11b^{high}F4/80^{+} cells confirm that these cells, respectively, have neutrophil and monocyte/macrophage morphology. *C*, Confocal image of day 8 LN section shows that CD11b^{high}F4/80^{+}CD11c^{-}CD169^{-} cells (magenta) are distinct from cells that bind the CD11c (green) and CD169 labels (double staining with CD11b (blue) or F4/80 (red) renders cells that bound green-tagged Ab yellow, turquoise, or white). Arrow in C1 magnification (*bottom*) highlights magenta CD11b^{high}F4/80^{+}CD11c^{-}CD169^{-} cells within medullary clusters of IgG1^{+} AFC white (*top*). White scale bar represents 200 μm in (*C*) and 50 μm in C1. *D*, Dot plots of FACS staining confirm that CD11b^{high}F4/80^{+} CD11c^{-}CD169^{-} cells (pink gate) are Gr1^{+}. Mean percentage ± SD from two independent experiments involving $n = 4$ mice in total is shown. *E*, The absolute number of Gr1^{high}CD11b^{high}F4/80^{-} neutrophils and Gr1^{int}CD11b^{high}F4/80^{+} monocytes/macrophages in LN treated day 0, 8, and 21 (*left*). Dot plots show the nonincorporation of BrdU by Gr1^{+}CD11b^{high} cells during the last 6 h before the LN were taken (*right*). Dot plots are representative of results obtained from $n = 9$ mice per time point studied in three independent experiments. Mean percentage of BrdU^{+} cells ± SD for all mice ($n = 9$) in each group is indicated. Statistically significant variations in the proportion of different cell populations between days 0 and 8 were assessed by Mann-Whitney nonparametric statistics (*B*, *D*, and *E*). ∗, $p < 0.01$, and ∗∗, $p < 0.001$.

Gr1^{high}CD11b^{high}F4/80^{-} neutrophils contained a high quantity of BAFF mRNA per cell, and CD169^{+} macrophages contained CXCL12 mRNA and protein (Fig. 4*D*). Nevertheless, these cells did not make a major contribution to the total production in LN of BAFF or CXCL12. This observation is in agreement with previous reports showing that BAFF and CXCL12 are produced by stromal cells (33, 34). Similarly, less than 20% of the TNF-α mRNA, known to be largely produced by lymphocytes, was produced by AFC-associated myeloid cells.

Microdissection confirms that the highest levels of mRNA for APRIL, TACI, BCMA, and CXCL12 in responding LN are found in the medulla

The previous experiments show a high level of APRIL mRNA produced by Gr1^{int}CD11b^{high}F4/80^{+} cells. Confocal microscopy indicates that these cells are present in the medullary cords where the most mature AFC are found. To confirm the local influence of AFC-associated cells in medullary cord tissue, we next used

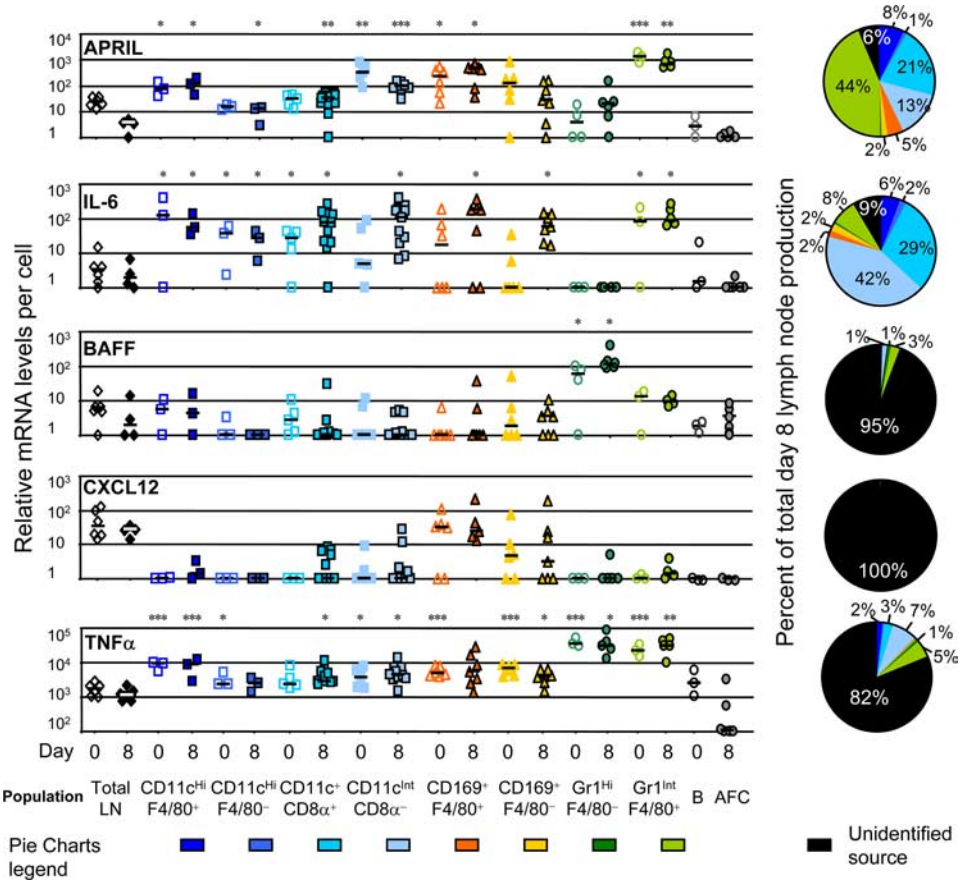

FIGURE 6. Analysis of mRNA encoding AFC survival factors reveals CD11c$^+$ DC as the main producers of IL-6, whereas Gr1^{int}CD11b^{high}F4/80$^+$ monocytes/macrophages are the principal source of APRIL. The transcription of genes encoding the main survival factors for AFC (TNF-α, BAFF, APRIL, IL-6, CXCL12) was quantified by real-time RT-PCR in total LN cell suspensions and FACS-sorted AFC-associated myeloid cell subsets. Expression at day 0 (open symbols) and day 8 (closed symbols) was compared. Each symbol represents an independent experiment performed from cells isolated from draining (day 8) or remote (day 0) LN from several mice. B = resting B cells. Horizontal bar shows geometric mean. Statistical significance of expressions higher in sorted cells vs total cell suspension at the corresponding time point was assessed by *t* test. ∗, $p < 0.05$; ∗∗, $p < 0.005$; and ∗∗∗, $p < 0.0005$. Pie charts represent an estimate of the relative contribution of each subset of myeloid cells to the total amount of transcript detected in the total cell suspension of day-8 LN. For each gene transcript, the percentage from unidentified source (black) represents the difference between the total amount of mRNA produced in day-8 total cell suspension and the sum of the mRNA produced by the different sorted myeloid cells. Pie charts populations are represented in the same color as for the mRNA produced by the sorted cells at day 8. Percentage values below 1% are not reported.

microdissection of day-8 LN and compared the relative mRNAs levels in different areas of the node. Three distinct regions identified by immunofluorescence confocal microscopy (as in Fig. 2*B*) remained identifiable in serial cresyl violet-stained sections, in which mRNA is preserved. This process allowed their microdissection without including other LN regions. The regions identified

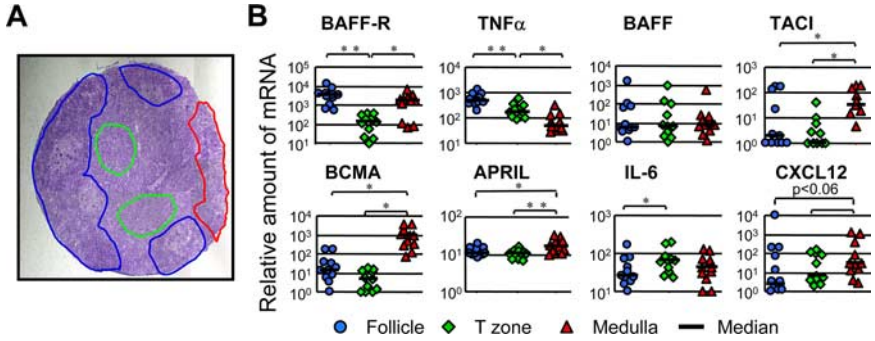

FIGURE 7. The polarization of AFC and factors that influence their growth, maturation and survival in LN. *A*, Composite view of a day-8 LN section stained with cresyl violet. The three distinct areas microdissected are delineated: the follicular mantle (blue), the T zone area (green), and the medulla (red). These were identified by confocal microscopy from serial sections stained showing cells adjacent to high endothelial venules (peripheral node addressin (PNAd)) and intranodal lymphatics (Lyve-1) as in Fig. 2*A*. *B*, Local expression of the indicated genes was quantified by real-time RT-PCR (dot plots). Each symbol represents the relative amount of mRNA obtained from one type of area after dissection of 20 to 40 serial sections from one LN. Eleven LN from $n = 11$ mice were assessed from four independent experiments. Statistical significance was assessed by paired *t* test; ∗, $p < 0.05$ for values between two groups linked by upper line and ∗∗, $p < 0.005$. For CXCL12, the statistical significance between the follicles and the T zone and the T zone and the medulla ($p < 0.06$) is marked.

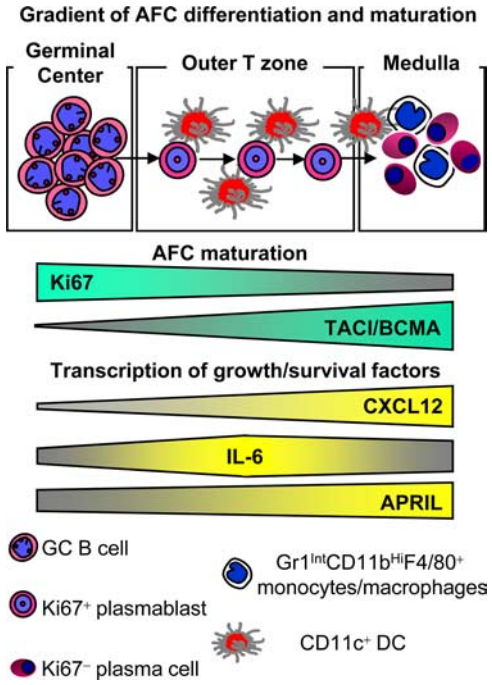

FIGURE 8. Sequential myeloid microenvironments encountered by the AFC during their extrafollicular maturation. By day 8 after immunization, $Ki67^+$ plasmablasts emerging from GC migrate along the outer edge of the T zone to the medulla. By the time they reach the medulla, most of these AFC have come out of cell cycle and are mature plasma cells. This migration is driven by a CXCL12 gradient that is sensed through the CXCR4 expressed by AFC. IL-6 is produced by $CD11c^+$ DC along the length of this migration pathway, but peaks in the T zone. The production of APRIL by myeloid cells, sensed by BCMA and TACI on AFC, is highest in the medulla where its production is attributable to $Gr1^{int}CD11b^{high}F4/80^+$ monocytes/macrophages.

were 1) the secondary follicles; 2) the central T zone, which is devoid of AFC; and 3) the medullary cords containing most of the mature AFC (Fig. 7*A*). The plasmablast-rich perivascular zones were not sufficiently well demarcated in cresyl violet-stained sections to allow their analysis by this approach.

The follicles had the highest levels of BAFF-R and TNF-α mRNA, consistent with the requirement of the signaling involving these proteins for GC formation or maintenance and B cell homeostasis (35, 36) (Fig. 7*B*). By contrast, BAFF expression was uniformly distributed throughout the three areas assessed.

The medullary areas contained around 30-fold more mRNA specific for TACI and 200-fold more mRNA for BCMA than the central T zone (Fig. 7*B*). This reflects the high frequency of AFC expressing these receptors in the medulla and AFC absence from the central T zone. It confirms that the areas of T zone dissected were not contaminated with AFC. As expected from the medullary location of $Gr1^{int}F4/80^+$ cells, the median level of APRIL in the medulla is almost twice (1.75-fold) that of the median level in the follicles and T zone ($p < 0.05$ and $p < 0.005$, respectively). The relatively low number of these cells is the likely reason that this increased expression in the medulla is relatively modest. Nevertheless $Gr1^{int}F4/80^+$ cells have a strategic location in that they are surrounded by AFC that do not produce APRIL (Fig. 6). Medullary CXCL12 mRNA is 4- and 10-fold higher than mRNA found in the T zone and follicles, respectively, although these differences just fail to reach significance ($p < 0.06$) (Fig. 7*B*, *right panels*) (for CXCL12 also see Allen et al. (37)).

Median expressions of IL-6 in the T zone and the medulla are 2.5- and 1.5-fold higher, respectively, than the median IL-6 expression in the follicles, but statistical significance is only reached for the T zone levels being higher than those in the follicles ($p < 0.05$). It seems likely that $CD11c^+$ DC in the central T zone are producing this IL-6 mRNA.

Taken together the range of approaches used in this study allow a picture to be built of the maturation gradient of AFC from the edge of the follicles along the perivascular zone to the medulla and their association with a range of cells that produce factors that influence their migration, maturation, and survival. This scenario is diagrammed in Fig. 8.

Discussion

The present study highlights major changes that occur in the path of plasmablast migration and differentiation into plasma cells during responses to alumNP-OVA in previously virgin LN. A range of myeloid-supporting cells populate these migration and differentiation sites. Both plasmablasts and plasma cells express the chemokine receptor CXCR4, which is necessary for their attraction to areas of the LN producing the corresponding chemokine CXCL12 (34). The similar expression of CXCR4 by many of the AFC-associated myeloid cells identified in the present study may in part explain their colocalization (see Supplemental Table III).[4] The proportion of AFC expressing Ki67 is greatest in the T zone adjacent to the base of the GC, and the proportion expressing this proliferation marker progressively falls the further they are located from the follicles. Thus AFC in the tips of the medullary cords are mainly postmitotic plasma cells. This occurrence may reflect the known associated increase in the expression of BLIMP-1, a key transcription factor in the maturation of AFC (38), and their exit from cell cycle (39). Microdissection of LN sections confirms that the concentration of CXCL12 in the medulla is higher than the concentration in the central T zone or follicles, providing a chemokine gradient directing this AFC migration (37) to the medulla where APRIL gene transcription is greatest (as shown in Fig. 7 and summarized in Fig. 8). Analysis of cells sorted from LN shows that the transcription of CXCL12 is minimal in most of the subsets of myeloid cells that associate with plasmablasts and plasma cells. Only the $CD169^+$ cells that are located beneath the lymphatic endothelium consistently produced CXCL12, but this is a negligible proportion of the nodal production of this cytokine; so the main production is most likely attributable to stromal cells (37).

The rapid loss of AFC from the node in the second and third week of the response (Fig. 1*A*) at least in part reflects local death in situ (4). This result is likely from more AFC being produced than can be sustained by the limited stroma able to support their long-term survival (8). This outcome may relate to the number of cells producing APRIL and IL-6 mRNA within the day-8 LN. Not all AFC fully mature and die in the LN. Some leave the node via the efferent lymph and settle in plasma cell-supporting niches in the bone marrow (5–7). There is evidence that up-regulation of the sphingosine-1-phosphate receptor-1 allows these cells to emigrate from the LN, attracted by the sphingosine-1-phosphate present in the lymph and blood circulation (40). The potential relationship between the availability of survival factors provided by the local environment in secondary lymphoid organs and the fate decision between sedentary vs migrant AFC remains to be investigated.

In the present study the production of the mRNA encoding the TNF family member APRIL was almost exclusively restricted to the AFC-associated myeloid cells identified. The highest local production was associated with $Gr1^{int}CD11b^{high}F4/80^+$ monocytes/macrophages that colonize the center of the medullary cords. This higher level of APRIL mRNA is likely to be associated with sufficient local APRIL protein production to cause its functional oligomerization (14). The strong up-regulation by AFC of the

APRIL and BAFF receptors, TACI and BCMA, makes it likely that the local production of APRIL influences AFC maturation and survival (Fig. 1*C*). The ability of APRIL in vitro is well documented (14, 15, 41). Unlike APRIL, BAFF is not produced by AFC-associated macrophages or DC. Both the $Gr1^{int}CD11b^{high}F4/80^{+}$ monocytes/macrophages and the $CD11c^{+}$ DC produced some TNF-α mRNA. TNF-α is a survival factor for AFC and a signal for neutrophils to release the BAFF protein stored in their Golgi (42, 43). Although some BAFF-producing $Gr1^{high}CD11b^{high}$ neutrophils were associated with AFC in the medullary cords, there are so few of these cells that they are unlikely to make a major contribution to nodal BAFF production.

The different myeloid cell subsets that align with AFC all increase in number during the first 8 days of the response to alum-precipitated OVA and the AFC-associated DC are induced to proliferate in situ. A number of T-dependent and T-independent signals are likely to operate in the attraction of AFC-associated myeloid cells and in their induction to proliferate and produce AFC growth and maturation factors. In the response we studied, a strong helper function, potentially through CD40L delivered by CD4 T cells, may induce the observed proliferation among $CD11c^{+}$ cells. This mechanism has been shown in mice given agonistic anti-CD40 Ab, a treatment that induces a massive expansion of plasmablast-associated $CD11c^{+}$ DC and greatly increases medullary plasma cell numbers and survival (10, 44). The $CD11c^{+}$ DC studied all express CD40, B7, and MHC class II molecules (see Supplemental Table III)[4] and consequently are equipped to make cognate interactions with primed CD4 T cells in the outer T zone (45). In addition, signals from CD4 T cells via CD40 ligation or cytokine secretion may promote APRIL expression (46) and contribute to the maturation of the microenvironment that supports Ab production. The close proximity of AFC-associated myeloid cells to the intranodal lymphatics positions them well to interact with lymph-borne soluble molecules such as cytokines and Ag (47). This interaction might include proliferation or activation of AFC-associated myeloid cells triggered through T-independent signals such as TLR stimulation (48, 49). In this case the production of APRIL may promote Ig class switching in outer T zone B blasts (46).

Overlapping activities among the range of factors that influence growth and survival, combined with the diversity of myeloid cells that produce these factors, may explain the partial effect on AFC production and function when a single subset of AFC-associated cells is depleted (16, 28, 50), or a single factor is absent (16, 21, 51, 52). This redundancy needs to be considered when attempts are made to suppress undesirable Ab responses by depleting factors that influence AFC growth, differentiation, or survival (53, 54). Despite this redundancy it seems likely that, in concert, the impressive range of cells that chaperone AFC plays a major role in influencing the quality, magnitude, and duration of the Ab responses.

Acknowledgments

We are grateful to Dagmar Scheel-Toellner, Cornelia Oetke, Paul Crocker, Vasileios Bekiaris, and Saba Shakib for helpful discussions or technical advice.

Disclosures

The authors have no financial conflict of interest.

References

1. Toellner, K. M., S. A. Luther, D. M. Sze, R. K. Choy, D. R. Taylor, I. C. MacLennan, and H. Acha-Orbea. 1998. T helper 1 (Th1) and Th2 characteristics start to develop during T cell priming and are associated with an immediate ability to induce immunoglobulin class switching. *J. Exp. Med.* 187: 1193–1204.
2. Liu, Y. J., J. Zhang, P. J. Lane, E. Y. Chan, and I. C. MacLennan. 1991. Sites of specific B cell activation in primary and secondary responses to T cell-dependent and T cell-independent antigens. *Eur. J. Immunol.* 21: 2951–2962.
3. Jacob, J., R. Kassir, and G. Kelsoe. 1991. In situ studies of the primary immune response to (4-hydroxy-3-nitrophenyl)acetyl. I. The architecture and dynamics of responding cell populations. *J. Exp. Med.* 173: 1165–1175.
4. Smith, K. G., T. D. Hewitson, G. J. Nossal, and D. M. Tarlinton. 1996. The phenotype and fate of the antibody-forming cells of the splenic foci. *Eur. J. Immunol.* 26: 444–448.
5. Manz, R. A., A. Thiel, and A. Radbruch. 1997. Lifetime of plasma cells in the bone marrow. *Nature* 388: 133–134.
6. Blink, E. J., A. Light, A. Kallies, S. L. Nutt, P. D. Hodgkin, and D. M. Tarlinton. 2005. Early appearance of germinal center-derived memory B cells and plasma cells in blood after primary immunization. *J. Exp. Med.* 201: 545–554.
7. Ho, F., J. E. Lortan, I. C. MacLennan, and M. Khan. 1986. Distinct short-lived and long-lived antibody-producing cell populations. *Eur. J. Immunol.* 16: 1297–1301.
8. Sze, D. M., K. M. Toellner, C. Garcia de Vinuesa, D. R. Taylor, and I. C. MacLennan. 2000. Intrinsic constraint on plasmablast growth and extrinsic limits of plasma cell survival. *J. Exp. Med.* 192: 813–821.
9. Garcia De Vinuesa, C., A. Gulbranson-Judge, M. Khan, P. O'Leary, M. Cascalho, M. Wabl, G. G. Klaus, M. J. Owen, and I. C. MacLennan. 1999. Dendritic cells associated with plasmablast survival. *Eur. J. Immunol.* 29: 3712–3721.
10. MacLennan, I. C., K. M. Toellner, A. F. Cunningham, K. Serre, D. M. Sze, E. Zuniga, M. C. Cook, and C. G. Vinuesa. 2003. Extrafollicular antibody responses. *Immunol. Rev.* 194: 8–18.
11. Minges Wols, H. A., G. H. Underhill, G. S. Kansas, and P. L. Witte. 2002. The role of bone marrow-derived stromal cells in the maintenance of plasma cell longevity. *J. Immunol.* 169: 4213–4221.
12. Cassese, G., S. Arce, A. E. Hauser, K. Lehnert, B. Moewes, M. Mostarac, G. Muehlinghaus, M. Szyska, A. Radbruch, and R. A. Manz. 2003. Plasma cell survival is mediated by synergistic effects of cytokines and adhesion-dependent signals. *J. Immunol.* 171: 1684–1690.
13. Suematsu, S., T. Matsuda, K. Aozasa, S. Akira, N. Nakano, S. Ohno, J. Miyazaki, K. Yamamura, T. Hirano, and T. Kishimoto. 1989. IgG1 plasmacytosis in interleukin 6 transgenic mice. *Proc. Natl. Acad. Sci. USA* 86: 7547–7551.
14. Bossen, C., T. G. Cachero, A. Tardivel, K. Ingold, L. Willen, M. Dobles, M. L. Scott, A. Maquelin, E. Belnoue, C. A. Siegrist, et al. 2008. TACI, unlike BAFF-R, is solely activated by oligomeric BAFF and APRIL to support survival of activated B cells and plasmablasts. *Blood* 111: 1004–1012.
15. Belnoue, E., M. Pihlgren, T. L. McGaha, C. Tougne, A. F. Rochat, C. Bossen, P. Schneider, B. Huard, P. H. Lambert, and C. A. Siegrist. 2008. APRIL is critical for plasmablast survival in the bone marrow and poorly expressed by early-life bone marrow stromal cells. *Blood* 111: 2755–2764.
16. Balazs, M., F. Martin, T. Zhou, and J. Kearney. 2002. Blood dendritic cells interact with splenic marginal zone B cells to initiate T-independent immune responses. *Immunity* 17: 341–352.
17. O'Connor, B. P., V. S. Raman, L. D. Erickson, W. J. Cook, L. K. Weaver, C. Ahonen, L. L. Lin, G. T. Mantchev, R. J. Bram, and R. J. Noelle. 2004. BCMA is essential for the survival of long-lived bone marrow plasma cells. *J. Exp. Med.* 199: 91–98.
18. Tangye, S. G., V. L. Bryant, A. K. Cuss, and K. L. Good. 2006. BAFF, APRIL and human B cell disorders. *Semin. Immunol.* 18: 305–317.
19. Nishimoto, N., and T. Kishimoto. 2006. Interleukin 6: from bench to bedside. *Nat. Clin. Pract. Rheumatol.* 2: 619–626.
20. Alsayed, Y., H. Ngo, J. Runnels, X. Leleu, U. K. Singha, C. M. Pitsillides, J. A. Spencer, T. Kimlinger, J. M. Ghobrial, X. Jia, et al. 2007. Mechanisms of regulation of CXCR4/SDF-1 (CXCL12)-dependent migration and homing in multiple myeloma. *Blood* 109: 2708–2717.
21. Moreaux, J., E. Legouffe, E. Jourdan, P. Quittet, T. Reme, C. Lugagne, P. Moine, J. F. Rossi, B. Klein, and K. Tarte. 2004. BAFF and APRIL protect myeloma cells from apoptosis induced by interleukin 6 deprivation and dexamethasone. *Blood* 103: 3148–3157.
22. Underhill, G. H., H. A. Minges Wols, J. L. Fornek, P. L. Witte, and G. S. Kansas. 2002. IgG plasma cells display a unique spectrum of leukocyte adhesion and homing molecules. *Blood* 99: 2905–2912.
23. Henri, S., D. Vremec, A. Kamath, J. Waithman, S. Williams, C. Benoist, K. Burnham, S. Saeland, E. Handman, and K. Shortman. 2001. The dendritic cell populations of mouse lymph nodes. *J. Immunol.* 167: 741–748.
24. Oetke, C., M. C. Vinson, C. Jones, and P. R. Crocker. 2006. Sialoadhesin-deficient mice exhibit subtle changes in B- and T-cell populations and reduced immunoglobulin M levels. *Mol. Cell Biol.* 26: 1549–1557.
25. Junt, T., E. A. Moseman, M. Iannacone, S. Massberg, P. A. Lang, M. Boes, K. Fink, S. E. Henrickson, D. M. Shayakhmetov, N. C. Di Paolo, et al. 2007. Subcapsular sinus macrophages in lymph nodes clear lymph-borne viruses and present them to antiviral B cells. *Nature* 450: 110–114.
26. Phan, T. G., I. Grigorova, T. Okada, and J. G. Cyster. 2007. Subcapsular encounter and complement-dependent transport of immune complexes by lymph node B cells. *Nat. Immunol.* 8: 992–1000.
27. Geissmann, F., S. Jung, and D. R. Littman. 2003. Blood monocytes consist of two principal subsets with distinct migratory properties. *Immunity* 19: 71–82.
28. Jordan, M. B., D. M. Mills, J. Kappler, P. Marrack, and J. C. Cambier. 2004. Promotion of B cell immune responses via an alum-induced myeloid cell population. *Science* 304: 1808–1810.

29. Nakano, H., M. Yanagita, and M. D. Gunn. 2001. CD11c$^+$B220$^+$Gr-1$^+$ cells in mouse lymph nodes and spleen display characteristics of plasmacytoid dendritic cells. *J. Exp. Med.* 194: 1171–1178.
30. Tacke, F., F. Ginhoux, C. Jakubzick, N. van Rooijen, M. Merad, and G. J. Randolph. 2006. Immature monocytes acquire antigens from other cells in the bone marrow and present them to T cells after maturing in the periphery. *J. Exp. Med.* 203: 583–597.
31. Wang, H. B., and P. F. Weller. 2008. Pivotal advance: eosinophils mediate early alum adjuvant-elicited B cell priming and IgM production. *J. Leukocyte Biol.* 83: 817–821.
32. Kool, M., T. Soullié, M. van Nimwegen, M. A. Willart, F. Muskens, S. Jung, H. C. Hoogsteden, H. Hammad, and B. N. Lambrecht. 2008. Alum adjuvant boosts adaptive immunity by inducing uric acid and activating inflammatory dendritic cells. *J. Exp. Med*. 205: 869–882.
33. Gorelik, L., K. Gilbride, M. Dobles, S. L. Kalled, D. Zandman, and M. L. Scott. 2003. Normal B cell homeostasis requires B cell activation factor production by radiation-resistant cells. *J. Exp. Med.* 198: 937–945.
34. Hargreaves, D. C., P. L. Hyman, T. T. Lu, V. N. Ngo, A. Bidgol, G. Suzuki, Y. R. Zou, D. R. Littman, and J. G. Cyster. 2001. A coordinated change in chemokine responsiveness guides plasma cell movements. *J. Exp. Med.* 194: 45–56.
35. Vora, K. A., L. C. Wang, S. P. Rao, Z. Y. Liu, G. R. Majeau, A. H. Cutler, P. S. Hochman, M. L. Scott, and S. L. Kalled. 2003. Cutting edge: germinal centers formed in the absence of B cell-activating factor belonging to the TNF family exhibit impaired maturation and function. *J. Immunol.* 171: 547–551.
36. Pasparakis, M., L. Alexopoulou, V. Episkopou, and G. Kollias. 1996. Immune and inflammatory responses in TNF α-deficient mice: a critical requirement for TNF α in the formation of primary B cell follicles, follicular dendritic cell networks and germinal centers, and in the maturation of the humoral immune response. *J. Exp. Med.* 184: 1397–1411.
37. Allen, C. D., K. M. Ansel, C. Low, R. Lesley, H. Tamamura, N. Fujii, and J. G. Cyster. 2004. Germinal center dark and light zone organization is mediated by CXCR4 and CXCR5. *Nat. Immunol.* 5: 943–952.
38. Kallies, A., J. Hasbold, D. M. Tarlinton, W. Dietrich, L. M. Corcoran, P. D. Hodgkin, and S. L. Nutt. 2004. Plasma cell ontogeny defined by quantitative changes in blimp-1 expression. *J. Exp. Med.* 200: 967–977.
39. Lin, Y., K. Wong, and K. Calame. 1997. Repression of c-myc transcription by Blimp-1, an inducer of terminal B cell differentiation. *Science* 276: 596–599.
40. Kabashima, K., N. M. Haynes, Y. Xu, S. L. Nutt, M. L. Allende, R. L. Proia, and J. G. Cyster. 2006. Plasma cell S1P1 expression determines secondary lymphoid organ retention versus bone marrow tropism. *J. Exp. Med.* 203: 2683–2690.
41. Ingold, K., A. Zumsteg, A. Tardivel, B. Huard, Q. G. Steiner, T. G. Cachero, F. Qiang, L. Gorelik, S. L. Kalled, H. Acha-Orbea, et al. 2005. Identification of proteoglycans as the APRIL-specific binding partners. *J. Exp. Med.* 201: 1375–1383.
42. Scapini, P., A. Carletto, B. Nardelli, F. Calzetti, V. Roschke, F. Merigo, N. Tamassia, S. Pieropan, D. Biasi, A. Sbarbati, et al. 2005. Proinflammatory mediators elicit secretion of the intracellular B-lymphocyte stimulator pool (BLyS) that is stored in activated neutrophils: implications for inflammatory diseases. *Blood* 105: 830–837.
43. Assi, L. K., S. H. Wong, A. Ludwig, K. Raza, C. Gordon, M. Salmon, J. M. Lord, and D. Scheel-Toellner. 2007. Tumor necrosis factor α activates release of B lymphocyte stimulator by neutrophils infiltrating the rheumatoid joint. *Arthritis Rheum.* 56: 1776–1786.
44. Garcia de Vinuesa, C., I. C. MacLennan, M. Holman, and G. G. Klaus. 1999. Anti-CD40 antibody enhances responses to polysaccharide without mimicking T cell help. *Eur. J. Immunol.* 29: 3216–3224.
45. Bajenoff, M., S. Granjeaud, and S. Guerder. 2003. The strategy of T cell antigen-presenting cell encounter in antigen-draining lymph nodes revealed by imaging of initial T cell activation. *J. Exp. Med.* 198: 715–724.
46. Litinskiy, M. B., B. Nardelli, D. M. Hilbert, B. He, A. Schaffer, P. Casali, and A. Cerutti. 2002. DCs induce CD40-independent immunoglobulin class switching through BLyS and APRIL. *Nat. Immunol.* 3: 822–829.
47. Gretz, J. E., C. C. Norbury, A. O. Anderson, A. E. Proudfoot, and S. Shaw. 2000. Lymph-borne chemokines and other low molecular weight molecules reach high endothelial venules via specialized conduits while a functional barrier limits access to the lymphocyte microenvironments in lymph node cortex. *J. Exp. Med.* 192: 1425–1440.
48. Hardenberg, G., L. Planelles, C. M. Schwarte, L. van Bostelen, T. Le Huong, M. Hahne, and J. P. Medema. 2007. Specific TLR ligands regulate APRIL secretion by dendritic cells in a PKR-dependent manner. *Eur. J. Immunol.* 37: 2900–2911.
49. Carmody, R. J., Q. Ruan, S. Palmer, B. Hilliard, and Y. H. Chen. 2007. Negative regulation of toll-like receptor signaling by NF-κB p50 ubiquitination blockade. *Science* 317: 675–678.
50. Hebel, K., K. Griewank, A. Inamine, H. D. Chang, B. Muller-Hilke, S. Fillatreau, R. A. Manz, A. Radbruch, and S. Jung. 2006. Plasma cell differentiation in T-independent type 2 immune responses is independent of CD11c^{high} dendritic cells. *Eur. J. Immunol.* 36: 2912–2919.
51. Kopf, M., H. Baumann, G. Freer, M. Freudenberg, M. Lamers, T. Kishimoto, R. Zinkernagel, H. Bluethmann, and G. Kohler. 1994. Impaired immune and acute-phase responses in interleukin-6-deficient mice. *Nature* 368: 339–342.
52. Nishio, M., T. Endo, N. Tsukada, J. Ohata, S. Kitada, J. C. Reed, N. J. Zvaifler, and T. J. Kipps. 2005. Nurselike cells express BAFF and APRIL, which can promote survival of chronic lymphocytic leukemia cells via a paracrine pathway distinct from that of SDF-1α. *Blood* 106: 1012–1020.
53. Anderson, K. C. 2007. Targeted therapy of multiple myeloma based upon tumor-microenvironmental interactions. *Exp. Hematol.* 35: 155–162.
54. Piazza, F. A., C. Gurrieri, L. Trentin, and G. Semenzato. 2007. Towards a new age in the treatment of multiple myeloma. *Ann. Hematol.* 86: 159–172.